

Optical control of topological memory based on orbital magnetization

Sergey S. Pershoguba¹ and Victor M. Yakovenko²

¹*Department of Physics and Astronomy, University of New Hampshire, Durham, New Hampshire 03824, USA*

²*JQI, Department of Physics, University of Maryland, College Park, Maryland 20742, USA*

(Dated: June 28, 2021)

Motivated by twisted graphene multilayers, we study interaction of a Chern insulator with circularly polarized light. The interaction energy contains an antisymmetric term that couples to the helicity of incident light. For a two-band Chern insulator, this term is expressed as an integral involving the Berry curvature of the system. Taking advantage of this interaction, we propose an experimental protocol for switching topological memory based on orbital magnetization by circularly polarized light and discuss its feasibility for the Chern insulators found in twisted graphene multilayers.

Introduction. There has been much interest in heterostructures of twisted graphene multilayers [1]. At a small interlayer twist angle $\sim 1^\circ$, they form a periodic moiré superlattice with a large unit cell size $a_m \sim 10$ nm and exhibit flat electronic energy bands [2]. Therefore these systems provide a versatile and highly-tunable platform for studying electron correlations. Among many interesting phases, Chern insulators were recently identified [3–7], which have a non-zero integer topological Chern number C and exhibit quantized Hall resistance R_H . They originate from spontaneous valley polarization induced by electronic correlations, resulting in orbital magnetization \mathbf{M} due to the incipient Berry curvature of graphene [8]. Experiments [3–7] have demonstrated that the sign of \mathbf{M} can be switched by weak pulses of electric or magnetic fields, or electric currents, thus realizing non-volatile topological memory [7].

In this Letter, we examine writing (and reading) of topological memory using optics. Consider circularly polarized light normally incident onto the surface of a Chern insulator, as shown in Fig. 1. Its helicity \mathbf{h} , parallel to the direction of light propagation, acts as an effective magnetic field. It couples to orbital magnetization \mathbf{M} of the Chern insulator, which is perpendicular to the layers. The sign of interaction energy is determined by $\mathbf{h} \cdot \mathbf{M}$, thus helicity of light makes one sign of \mathbf{M} energetically favorable, which can switch the memory.

Magnetization reversal by pulsed circularly polarized laser radiation was first demonstrated in GdFeCo magnetic films [9]. However, microscopic mechanism of this effect in spin-based magnets is subject to debate [10]. Here we focus on Chern insulators, expecting stronger electric-dipole coupling to light due to their orbital nature. The interaction between orbital magnetization and circularly polarized light is general and not limited to twisted graphene multilayers. There have been extensive studies of valley-selective optics in transition metal dichalcogenides [11]. The ac Stark shift of the exciton energy was observed in WSe₂ [12] and WS₂ [13], as well as the Bloch-Siegert shift in WS₂ [14]. Recently, spontaneous valley polarization was observed in the AB-stacked MoTe₂/WSe₂ bilayers [15], reminiscent of the similar phenomenon in twisted graphene multilayers.

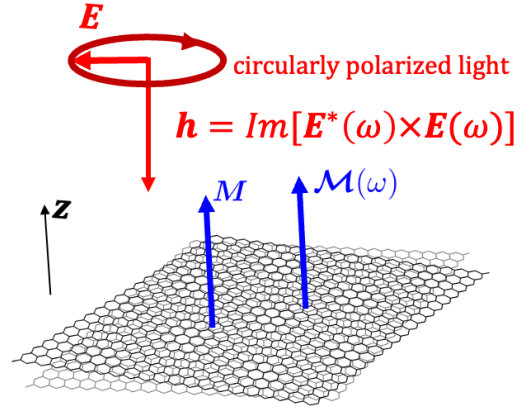


FIG. 1. Experimental setup for controlling orbital magnetization \mathbf{M} of a Chern insulator by circularly polarized light.

We start with a symmetry analysis of the ac Stark effect, followed by a proposed experimental protocol. Then we present microscopic calculations for a two-band model and express optical response in terms of the Berry curvature and Chern number. We conclude with applications to twisted graphene multilayers.

Symmetry analysis. Suppose a monochromatic ac electric field $\mathbf{E}(t) = [\mathbf{E}(\omega)e^{-i\omega t} + \mathbf{E}(-\omega)e^{i\omega t}]/2$, where $\mathbf{E}(-\omega) = \mathbf{E}^*(\omega)$, is applied to the system. The ac Stark effect [16–18] is the corresponding change U of the energy of the system

$$U = -\frac{1}{4}\text{Re}[\chi^{\alpha\beta}(\omega)E_\alpha(-\omega)E_\beta(\omega)] \equiv U_s + U_a, \quad (1)$$

It is expressed in terms of the dynamical polarizability tensor $\chi^{\alpha\beta}(\omega)$, where α and β are the Cartesian indices in three dimensions (3D) (see details in Sec. I of Supplemental Material [19]). It can be expanded into into symmetric $\chi_s^{\alpha\beta} = (\chi^{\alpha\beta} + \chi^{\beta\alpha})/2$ and antisymmetric $\chi_a^{\alpha\beta} = (\chi^{\alpha\beta} - \chi^{\beta\alpha})/2$ parts, thus generating the corresponding contributions U_s and U_a to the energy shift

$$U_s = -\frac{1}{4}\text{Re}[E_\alpha^*(\omega)E_\beta(\omega)]\text{Re}[\chi_s^{\alpha\beta}(\omega)], \quad (2)$$

$$U_a = \frac{1}{4}\text{Im}[E_\alpha^*(\omega)E_\beta(\omega)]\text{Im}[\chi_a^{\alpha\beta}(\omega)]. \quad (3)$$

The symmetric contribution U_s represents the conventional ac Stark energy shift [16–18] of no interest to us. The antisymmetric contribution U_a is less common and is permitted only in the systems with broken time-reversal symmetry. The symmetric tensor $\text{Re } \chi_s^{\alpha\beta}(\omega) = \text{Re } \chi_s^{\alpha\beta}(-\omega)$ is even, whereas the antisymmetric tensor $\text{Im } \chi_a^{\alpha\beta}(\omega) = -\text{Im } \chi_a^{\alpha\beta}(-\omega)$ is odd upon time reversal [20]. Pitaevskii [21] noted the antisymmetric part $\chi_a^{\alpha\beta}$ in the presence of an external magnetic field. The recently discovered orbital Chern insulators [3–7] break time-reversal symmetry spontaneously and, thus, should have a non-zero $\chi_a^{\alpha\beta}$, which is the subject of our work. It is instructive to represent the antisymmetric tensor $\chi_a^{\alpha\beta}(\omega)$ via a dual vector $\mathcal{M}(\omega)$

$$\chi_a^{\alpha\beta}(\omega) = -i \epsilon^{\alpha\beta\gamma} \mathcal{M}_\gamma(\omega), \quad (4)$$

where $\epsilon^{\alpha\beta\gamma}$ is the totally antisymmetric tensor in 3D. Then the corresponding energy contribution is

$$U_a = -\frac{1}{4} \text{Im} [\mathbf{E}^*(\omega) \times \mathbf{E}(\omega)] \cdot \text{Re } \mathcal{M}(\omega). \quad (5)$$

Since $\text{Re } \mathcal{M}(\omega)$ is an odd function of frequency ω , we can write it at low ω as $\text{Re } \mathcal{M}(\omega) \approx \omega \mathcal{M}'(0)$. Thus, in time domain for slowly changing $\mathbf{E}(t)$, Eq. (5) becomes

$$U_a = \frac{1}{2} \langle \partial_t \mathbf{E}(t) \times \mathbf{E}(t) \rangle_t \cdot \mathcal{M}'(0), \quad (6)$$

where $\langle \dots \rangle_t$ denotes time averaging. Equations (5) and (6) show that the sign of the energy U_a is determined by the scalar product of the vector $\mathcal{M}(\omega)$ characterizing the system and the helicity $\mathbf{h} = \text{Im} [\mathbf{E}^*(\omega) \times \mathbf{E}(\omega)] \parallel [\mathbf{E}(t) \times \partial_t \mathbf{E}(t)]$ of circularly polarized electric field. The vector $\mathcal{M}(\omega)$ is a time-reversal-odd axial vector, so it has the same symmetry as the static magnetization \mathbf{M} of the system. Both $\mathcal{M}(\omega)$ and \mathbf{M} originate from the Berry curvature (as derived later in the paper), but they are not equivalent. For two-dimensional (2D) twisted graphene multilayers, the vectors \mathbf{M} and $\mathcal{M} = \mathcal{M}\hat{z}$ are parallel to z axis in Fig. 1, so Eq. (5) becomes $U_a = -\text{Re}[\mathcal{M}(\omega)] \text{Im} [\mathbf{E}^*(\omega) \times \mathbf{E}(\omega)]_z / 4$. Below we present an experimental protocol for optical control of the sign of orbital magnetization that does not involve a quantitative estimate of $\mathcal{M}(\omega)$.

Experimental protocol. The Chern insulator state develops in the second-order phase transition at $T_c \approx 7.5$ K [7], where the system spontaneously breaks time-reversal symmetry. Either \mathcal{M} or \mathbf{M} or the Hall resistance R_H can be taken as the order parameter, having positive or negative sign. The experimentally measured sign of R_H can represent topological memory.

We propose to irradiate the system by circularly polarized light, which is likely to produce heating and raise the sample temperature T above T_c . So, we suggest to take advantage of this parasitic heating and use laser power to control T following the protocol sketched in

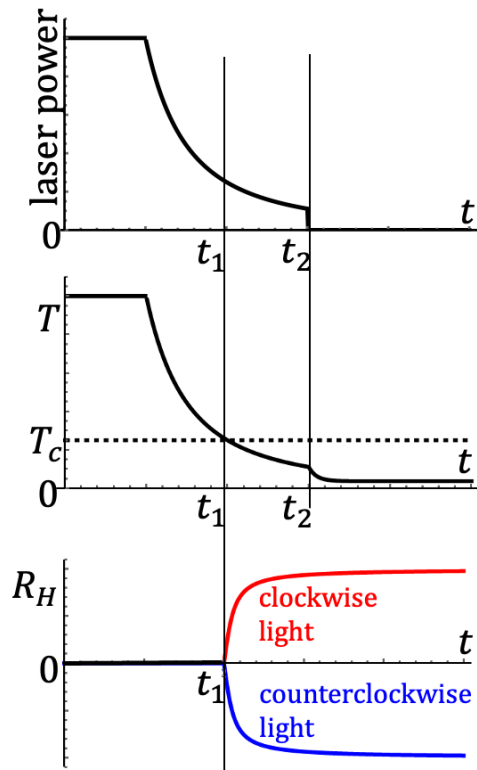


FIG. 2. Experimental protocol, showing laser power, the sample temperature T , and the Hall resistance R_H versus time t . Decreasing laser power lowers T and drives the sample through a transition at T_c . The sign of the resultant R_H is determined by the helicity of circularly polarized light.

Fig. 2. The three panels show laser power, the sample temperature T , and the Hall resistance R_H versus time t of the experiment.

At $t = 0$, we start at a high laser power, so that $T > T_c$ and $R_H = 0$. Then we gradually decrease laser power, which lowers T until it reaches T_c at $t = t_1$, where the sample undergoes a transition into the Chern insulator phase. The presence of circularly polarized light breaks symmetry between the two, otherwise equienergetic, states of the system characterized by opposite signs of R_H . The system chooses the state of lower energy U_a , as determined by helicity of incident light in Eq. (5), which is manifested in the sign of the measured R_H . Since the Landau energy at the second-order phase transition is quadratic in \mathcal{M} , whereas U_a is linear in \mathcal{M} , even a weak electric field \mathbf{E} in Eq. (5) is sufficient to control symmetry breaking. Once T decreases well below T_c , laser power can be turned off at $t = t_2$, but the sign of R_H stays the same.

Effectively, the circularly polarized light acts as a “training field” that forces the system to choose a particular sign during symmetry breaking. It is similar to a small training magnetic field applied to control the sign of spontaneously developing polar Kerr effect at the

superconducting transition in Sr_2RuO_4 , which breaks time-reversal symmetry [22]. The read-out of the sign of R_H in the Chern insulator can also be carried out optically by measuring the polar Kerr effect.

Microscopic derivation. Here we present a microscopic derivation of the magnetic vector $\mathcal{M}(\omega)$ appearing in Eq. (5). We start with a generic Hamiltonian $H = H_0 + V(t)$, consisting of the bare term H_0 and the time-dependent term $V(t) = e\mathbf{r} \cdot \mathbf{E}(t)$, which represents dipolar coupling to an oscillating electric field $\mathbf{E}(t)$. The operator \mathbf{r} here is either the coordinate of a single electron, e.g., for an atom, or the sum of coordinates for many electrons, e.g., in a crystal. The symmetric and antisymmetric parts of the polarizability tensor have the following form (see details in Secs. I and II of Supplemental Material [19])

$$\chi_s^{\alpha\beta}(\omega) = \sum_{\substack{m \in \{\text{emp}\} \\ n \in \{\text{occ}\}}} \frac{2e^2(\varepsilon_n - \varepsilon_m) \text{Re}(r_{nm}^\alpha r_{mn}^\beta)}{(\varepsilon_n - \varepsilon_m)^2 - (\hbar\omega + i\delta)^2},$$

$$\chi_a^{\alpha\beta}(\omega) = \sum_{\substack{m \in \{\text{emp}\} \\ n \in \{\text{occ}\}}} \frac{2ie^2\hbar\omega \text{Im}(r_{nm}^\alpha r_{mn}^\beta)}{(\varepsilon_n - \varepsilon_m)^2 - (\hbar\omega + i\delta)^2}. \quad (7)$$

Here the double summation runs over the occupied and empty electronic states of the energies ε_n and ε_m labeled by the indices n and m , respectively. The matrix elements of the coordinate r_{mn}^α are evaluated with respect to these states. The small parameter $\delta > 0$ simulates adiabatic onset of $V(t)$. The symmetric tensor $\chi_s^{\alpha\beta}(\omega)$ reproduces the conventional ac Stark energy shift [16–18], whereas we focus on the antisymmetric tensor $\chi_a^{\alpha\beta}(\omega)$. Equations (7) are written for $T = 0$, but can be easily generalized to non-zero temperature by introducing the Fermi occupation functions.

Now let us simplify $\chi_a^{\alpha\beta}(\omega)$ in Eq. (7) for a two-band crystalline Chern insulator (details are given in Sec. III of Supplemental Material [19]). In this case, the single-particle states are indexed by the quasimomentum \mathbf{k} and the indices v and c for the occupied valence band and the empty conduction band. The corresponding eigenenergies and Bloch wavefunctions are $\varepsilon_{v(c)}(\mathbf{k})$ and $\psi_{v(c),\mathbf{k}}(\mathbf{r}) = e^{i\mathbf{k}\mathbf{r}} u_{v(c),\mathbf{k}}(\mathbf{r})$. We do not write the spin index explicitly, so summation over the two spin orientations should be added to the final results. For a spatially-uniform electric field $\mathbf{E}(t)$, the perturbation $V(t)$ has only “vertical” interband matrix elements between the states ψ_{v,\mathbf{k}_1} and ψ_{c,\mathbf{k}_2} with $\mathbf{k}_1 = \mathbf{k}_2$. It is well known [23, 24] that these matrix elements represent the interband Berry connections, i.e., $r_{vc}^\alpha(\mathbf{k}) = i\langle u_{v,\mathbf{k}} | \partial^\alpha | u_{c,\mathbf{k}} \rangle$, where $\partial^\alpha = \partial/\partial k_\alpha$ denotes the momentum derivative. Furthermore, the antisymmetric product of the two matrix elements $\text{Im}[r_{vc}^\alpha r_{cv}^\beta] = -\varepsilon^{\alpha\beta\gamma} \Omega_{v,\gamma}(\mathbf{k})/2$ is expressed via the Berry curvature of the occupied band $\Omega_{v,\gamma}(\mathbf{k}) = i\varepsilon_{\alpha\beta\gamma} \langle \partial^\alpha u_{v,\mathbf{k}} | \partial^\beta u_{v,\mathbf{k}} \rangle$. For a planar 2D system, both the Berry vector $\boldsymbol{\Omega}_v =$

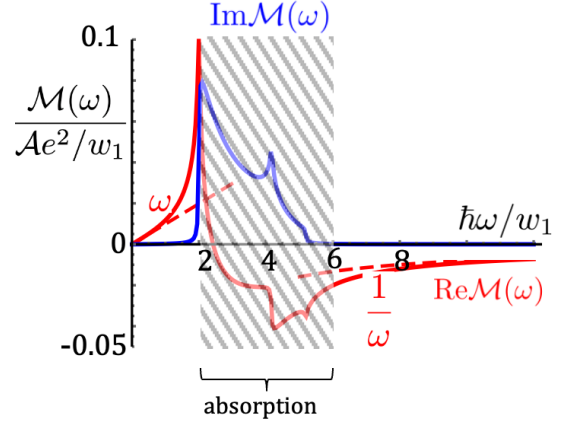


FIG. 3. Frequency dependence of $\mathcal{M}(\omega)$ in Eq. (5) for the antisymmetric ac Stark effect, calculated from Eq. (8) for the Haldane model with $C = 1$. The low and high frequency asymptotes from Eqs. (9) and (10) are shown by dashed lines.

$\Omega_v \hat{\mathbf{z}}$ and the magnetic vector $\mathcal{M}(\omega)$ in Eq. (4) are parallel to z axis. Thus we obtain from Eq. (7)

$$\frac{\mathcal{M}(\omega)}{\mathcal{A}} = \int \frac{d^2k}{(2\pi)^2} \frac{e^2 \hbar\omega \Omega_v(\mathbf{k})}{[\varepsilon_c(\mathbf{k}) - \varepsilon_v(\mathbf{k})]^2 - (\hbar\omega + i\delta)^2}, \quad (8)$$

where \mathcal{A} is the area of the system.

Let us examine the asymptotic behavior of Eq. (8) at low and high frequencies. At low subgap frequencies $\hbar\omega \ll \varepsilon_c(\mathbf{k}) - \varepsilon_v(\mathbf{k})$, we can drop ω in the denominator

$$\frac{\mathcal{M}(\omega)}{\mathcal{A}} \approx \hbar\omega \int \frac{d^2k}{(2\pi)^2} \frac{e^2 \Omega_v(\mathbf{k})}{[\varepsilon_c(\mathbf{k}) - \varepsilon_v(\mathbf{k})]^2}. \quad (9)$$

The integral in Eq. (9) gives $\mathcal{M}'(0)$, in Eq. (6).

At high frequencies $\hbar\omega \gg \varepsilon_c(\mathbf{k}) - \varepsilon_v(\mathbf{k})$, we find

$$\frac{\mathcal{M}(\omega)}{\mathcal{A}} \approx -\frac{e^2}{2\pi} \left(\frac{C}{\hbar\omega} + \frac{D}{(\hbar\omega)^3} \right), \quad (10)$$

$$C = \int \frac{d^2k}{2\pi} \Omega_v(\mathbf{k}), \quad D = \int \frac{d^2k}{2\pi} \Omega_v(\mathbf{k}) [\varepsilon_c(\mathbf{k}) - \varepsilon_v(\mathbf{k})]^2.$$

Comparing Eqs. (9) and (10), we observe that $\mathcal{M}(\omega)$ has opposite signs in the low and high frequency limits. Interestingly, the leading term C/ω in Eq. (10) depends only on the integer topological Chern number C , which determines the quantized Hall conductance $R_H^{-1} = -Ce^2/h$ of the edge states. If the Chern number vanishes, $C = 0$, then the leading term is D/ω^3 , consistent with earlier calculations [25, 26] of the bulk ac Hall conductivity $\sigma_H(\omega)$ for a two-band model. The interplay between edge and bulk contributions is discussed in Sec. IV of Supplemental Material [19].

At intermediate frequencies, the energy denominator in Eq. (8) may vanish at $\hbar\omega = \varepsilon_c(\mathbf{k}) - \varepsilon_v(\mathbf{k})$, thus producing an imaginary part of $\mathcal{M}(\omega)$, which physically represents resonant interband transitions with absorption of photons. $\text{Im}\mathcal{M}(\omega)$ depends on the magnetic

state of the system via the Berry curvature and can be measured by taking the difference between absorption rates for the two opposite circular polarizations. By Kramers-Kronig relation from Eq. (10), the imaginary part of $\mathcal{M}(\omega)$ satisfies a remarkable optical sum rule [27] in terms of the integer topological Chern number C

$$\int_{-\infty}^{\infty} d\omega \frac{\text{Im} \mathcal{M}(\omega)}{\mathcal{A}} = \frac{e^2}{2\hbar} C \quad (11)$$

(see details in Sec. III of Supplemental Material [19]).

As an illustration, the real and imaginary parts of $\mathcal{M}(\omega)$, calculated from Eq. (8) for the well-known Haldane model [28], are shown in Fig. 3 (details are given in Sec. V of Supplemental Material [19]). At low and high frequencies, the ω and $1/\omega$ asymptotic behavior from Eqs. (9) and (10) is indicated. At the intermediate frequencies where resonant absorption is possible, $\text{Re}\mathcal{M}(\omega)$ and $\text{Im}\mathcal{M}(\omega)$ exhibits a series of kinks and dips associated with band edges and van Hove singularities in the density of states.

The static orbital magnetization M of a Chern insulator can also be expressed as an integral involving the Berry curvature [29, 30]. However, the integrals for M and for $\mathcal{M}(\omega)$ in Eq. (8) are different. Thus, M and $\mathcal{M}(\omega)$ are not equivalent, but their signs are both determined by the sign of the Berry curvature $\Omega_v(\mathbf{k})$.

Application to twisted graphene multilayers. We consider a twisted graphene bilayer on the boron nitride (BN) substrate and follow the interpretation presented in Ref. [6] on the basis of theoretical models [8, 31, 32]. The staggered sublattice potential induced by the BN substrate separates the valence and conduction bands of graphene by the energy gap 2Δ and generates a non-zero Berry curvature near the K and K' points. The periodic potential produced by the moiré superlattice folds the valence and conduction bands into mini-bands at the K and K' valleys, where the lowest mini-bands acquire the Chern number $C = \pm 1$. At the filling factor $\nu = 4$ per moiré unit cell, the four mini-bands in the conduction band are fully occupied (for valleys K and K' , and spins up and down), so the system is a trivial band insulator. In contrast, at $\nu = 3$, Coulomb interaction between electrons induces spontaneous valley polarization. In that state, the two mini-bands, e.g., of the K' valley are fully occupied, whereas one mini-band of the K valley rises above the Fermi level and becomes empty (see Fig. 1(c) in Ref. [6]). This empty mini-band and the corresponding filled mini-band in the valence band, treated within a two-band model, experience the ac Stark energy shift U_a in Eq. (5) due to the Berry curvature in Eq. (8). By properly choosing the sign of helicity of circularly polarized light, it is possible to raise the energy U_a of this valley configuration and make it energetically unfavorable, thus forcing a spontaneous switch to the opposite valley polarization. (A more detailed discussion of valley-selective optics is presented in Sec. VI of Supplemental Material [19].)

Let us crudely estimate the magnitude of the proposed effect. Given that $\mathcal{M}(\omega)$ decreases both at low and high frequencies in Eqs. (9) and (10), the maximal $\mathcal{M}(\omega)$ is achieved at the optimal frequency of the order of bandgap, i.e., at $\hbar\omega \sim \Delta$. Then the antisymmetric ac Stark energy shift per unit cell \tilde{U}_a can be estimated as $\tilde{U}_a \sim (eEa_m)^2 C / 4\pi\Delta$ at the optimal frequency, where a_m is the moiré unit cell size. Taking the characteristic values $\Delta \sim 1$ meV, $a_m \sim 10$ nm, $C = 1$, and $E = 3 \times 10^4$ V/m (for a 0.01 W laser with the spot size $d = 0.1$ mm), we find the Stark energy $\tilde{U}_a^{(1)} \sim 8 \times 10^{-6}$ eV. For a laser of visible light $\hbar\omega \sim 2$ eV, this estimate is reduced by a factor of $\Delta/\hbar\omega \sim 5 \times 10^{-4}$ from Eq. (10), thus producing $\tilde{U}_a^{(2)} \sim 4 \times 10^{-9}$ eV. In comparison, the typical energy shift due to a magnetic field is $\mu_B B \sim 5.8 \times 10^{-5}$ eV $\times B[T]$ per unit cell carrying a magnetic moment of the order of Bohr magneton [7]. Thus, the two estimates $\tilde{U}_a^{(1)}$ and $\tilde{U}_a^{(2)}$ correspond to the effective magnetic fields $B^{(1)} \sim 0.1$ T and $B^{(2)} \sim 0.6$ G, respectively. Experimentally [7], magnetization was switched by a magnetic field as low as $B = 0.08$ T. So, the effect of circularly polarized light is comparable to the magnetic fields used in experiments [6, 7] to control magnetization. With a much higher pulsed laser power, an effective magnetic field about 50 T has been achieved in the optical Stark effect in transition metal dichalcogenides [12–14].

Conclusions. For the systems that break time-reversal symmetry, the energy of interaction with an external ac electric field $\mathbf{E}(\omega)$ contains an antisymmetric term U_a in Eq. (5) that couples to the helicity of circularly polarized light $\mathbf{h} = \text{Im}[\mathbf{E}^*(\omega) \times \mathbf{E}(\omega)]$. For a two-band Chern insulator, the coefficient $\mathcal{M}(\omega)$ in Eq. (5) is expressed as an integral over the Brillouin zone (8) involving the Berry curvature $\Omega_v(\mathbf{k})$ of the occupied valence band. Taking advantage of this interaction energy U_a , we propose an experimental protocol for switching the orbital magnetization of a Chern insulator using circularly polarized light as shown in Fig. 2. A gradual decrease of laser power lowers the sample temperature from $T > T_c$ to $T < T_c$ and drives the system through the time-reversal breaking transition at T_c . The helicity of circularly polarized light forces the system to select a particular sign of the orbital magnetization and the spontaneous Hall resistance R_H at the transition. Alternatively, applying circularly polarized light of the appropriate helicity at a low temperature, it is possible to raise the energy of a given spontaneous valley polarization and make it energetically unfavorable, thus forcing a switch to the opposite valley polarization. Both mechanisms realize optical control of topological memory based on spontaneous orbital magnetization.

We thank G. Polshyn for stimulating discussions that motivated this work. SP was supported by the U.S. Department of Energy (DOE), Office of Science, Basic Energy Sciences (BES) under Award No. DE-SC0020221.

-
- [1] E. Y. Andrei, D. K. Efetov, P. Jarillo-Herrero, A. H. MacDonald, K. F. Mak, T. Senthil, E. Tutuc, A. Yazdani, and A. F. Young, “The marvels of moiré materials,” *Nat. Rev. Mat.* **6**, 201 (2021).
- [2] R. Bistritzer and A. H. MacDonald, “Moiré bands in twisted double-layer graphene,” *PNAS* **108**, 12233 (2011).
- [3] X. Lu, P. Stepanov, W. Yang, M. Xie, A. M. Ali, I. Das, C. Urgell, C. Watanabe, T. Taniguchi, G. Zhang, A. Bachtold, A. MacDonald, and D. K. Efetov, “Superconductors, orbital magnets and correlated states in magic-angle bilayer graphene,” *Nature* **574**, 653 (2019).
- [4] A. L. Sharpe, E. J. Fox, A. W. Barnard, J. Finney, K. Watanabe, T. Taniguchi, M. A. Kastner, and D. Goldhaber-Gordon, “Emergent ferromagnetism near three-quarters filling in twisted bilayer graphene,” *Science* **365**, 605 (2019).
- [5] G. Chen, A. L. Sharpe, E. J. Fox, Y.-H. Zhang, S. Wang, L. Jiang, B. Lyu, H. Li, K. Watanabe, T. Taniguchi, Z. Shi, T. Senthil, D. Goldhaber-Gordon, Y. Zhang, and F. Wang, “Tunable correlated Chern insulator and ferromagnetism in a moiré superlattice,” *Nature* **579**, 56 (2020).
- [6] M. Serlin, C. L. Tschirhart, H. Polshyn, Y. Zhang, J. Zhu, K. Watanabe, T. Taniguchi, L. Balents, and A. F. Young, “Intrinsic quantized anomalous Hall effect in a moiré heterostructure,” *Science* **367**, 900 (2020).
- [7] H. Polshyn, J. Zhu, M. A. Kumar, Y. Zhang, F. Yang, C. L. Tschirhart, M. Serlin, K. Watanabe, T. Taniguchi, A. H. MacDonald, and A. F. Young, “Electrical switching of magnetic order in an orbital Chern insulator,” *Nature* **588**, 66 (2020).
- [8] J. C. W. Song, P. Samutpraphoot, and L. S. Levitov, “Topological Bloch bands in graphene superlattices,” *PNAS* **112**, 10879 (2015).
- [9] C. D. Stanciu, F. Hansteen, A. V. Kimel, A. Kirilyuk, A. Tsukamoto, A. Itoh, and Th. Rasing, “All-Optical Magnetic Recording with Circularly Polarized Light,” *Phys. Rev. Lett.* **99**, 047601 (2007).
- [10] E. Y. Vedmedenko, R. K. Kawakami, D. D. Sheka, P. Gambardella, A. Kirilyuk, A. Hirohata, C. Binek, O. Chubykalo-Fesenko, S. Sanvito, B. J. Kirby, J. Grollier, K. Everschor-Sitte, T. Kampfrath, C.-Y. You, and A. Berger, “The 2020 magnetism roadmap,” *J. Phys. D: Appl. Phys.* **53**, 453001 (2020).
- [11] K. F. Mak, D. Xiao, and J. Shan, “Light-valley interactions in 2D semiconductors,” *Nat. Photonics* **12**, 451 (2018).
- [12] J. Kim, X. Hong, C. Jin, S.-F. Shi, C.-Y. S. Chang, M.-H. Chiu, L.-J. Li, and F. Wang, “Ultrafast generation of pseudo-magnetic field for valley excitons in WSe_2 monolayers,” *Science* **346**, 1205 (2014).
- [13] E. J. Sie, J. W. McIver, Y.-H. Lee, L. Fu, J. Kong, and N. Gedik, “Valley-selective optical Stark effect in monolayer WS_2 ,” *Nat. Mat.* **14**, 290 (2015).
- [14] E. J. Sie, C. H. Lui, Y.-H. Lee, L. Fu, J. Kong, and N. Gedik, “Large, valley-exclusive Bloch-Siegert shift in monolayer WS_2 ,” *Science* **355**, 1066 (2017).
- [15] K. F. Mak, conference presentation, 14 June 2021.
- [16] N. B. Delone and V. P. Krainov, “AC Stark shift of atomic energy levels,” *Phys.-Usp.* **42**, 669 (1999).
- [17] M. Haas, U. D. Jentschura, and C. H. Keitel, “Comparison of classical and second quantized description of the dynamic Stark shift,” *Am. J. Phys.* **74**, 77 (2006).
- [18] D. H. Kobe, “Gauge invariant derivation of the AC Stark shift,” *J. Phys. B: Atom. Mol. Phys.* **16**, 1159 (1983).
- [19] Supplemental Material is available at “hyperlink generated by APS”.
- [20] L. D. Landau and E. M. Lifshitz, *Statistical Physics Part 1. Course of Theoretical Physics*, 3rd ed., Vol. 5 (Butterworth-Heinemann, 1980).
- [21] L. P. Pitaevskii, “Electric forces in a transparent dispersive medium,” *Sov. Phys. JETP* **12**, 1008 (1961).
- [22] J. Xia, Y. Maeno, P. T. Beyersdorf, M. M. Fejer, and A. Kapitulnik, “High Resolution Polar Kerr Effect Measurements of Sr_2RuO_4 : Evidence for Broken Time-Reversal Symmetry in the Superconducting State,” *Phys. Rev. Lett.* **97**, 167002 (2006).
- [23] E. I. Blount, *Formalisms of Band Theory in Solid State Physics*, edited by F. Seitz and D. Turnbull, Vol. 13 (Academic Press, New York and London, 1962).
- [24] E. M. Lifshitz and L. P. Pitaevskii, *Statistical Physics Part 2. Landau and Lifshitz Course of Theoretical Physics*, Vol. 9 (Pergamon Press, 1980).
- [25] Y. Yao, L. Kleinman, A. H. MacDonald, J. Sinova, T. Jungwirth, D.-S. Wang, E. Wang, and Q. Niu, “First Principles Calculation of Anomalous Hall Conductivity in Ferromagnetic bcc Fe,” *Phys. Rev. Lett.* **92**, 037204 (2004).
- [26] S. Tewari, C. Zhang, V. M. Yakovenko, and S. Das Sarma, “Time-Reversal Symmetry Breaking by a ($d + id$) Density-Wave State in Underdoped Cuprate Superconductors,” *Phys. Rev. Lett.* **100**, 217004 (2008).
- [27] W. Yao, D. Xiao, and Q. Niu, “Valley-dependent optoelectronics from inversion symmetry breaking,” *Phys. Rev. B* **77**, 235406 (2008).
- [28] F. D. M. Haldane, “Model for a Quantum Hall Effect without Landau Levels: Condensed-Matter Realization of the “Parity Anomaly”,” *Phys. Rev. Lett.* **61**, 2015 (1988).
- [29] D. Xiao, J. Shi, and Q. Niu, “Berry Phase Correction to Electron Density of States in Solids,” *Phys. Rev. Lett.* **95**, 137204 (2005).
- [30] T. Thonhauser, D. Ceresoli, D. Vanderbilt, and R. Resta, “Orbital Magnetization in Periodic Insulators,” *Phys. Rev. Lett.* **95**, 137205 (2005).
- [31] Y.-H. Zhang, D. Mao, and T. Senthil, “Twisted bilayer graphene aligned with hexagonal boron nitride: Anomalous Hall effect and a lattice model,” *Phys. Rev. Research* **1**, 033126 (2019).
- [32] N. Bultinck, S. Chatterjee, and M. P. Zaletel, “Mechanism for Anomalous Hall Ferromagnetism in Twisted Bilayer Graphene,” *Phys. Rev. Lett.* **124**, 166601 (2020).